Engineering Structures 264 (2022) 114423

Contents lists available at ScienceDirect

Engineering Structures

journal homepage: www.elsevier.com/locate/engstruct

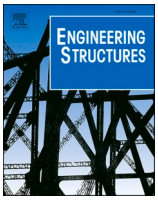

Computationally aware estimation of ultimate strength reduction of stiffened panels caused by welding residual stress: From finite element to data-driven methods

Shen Li [a], Andrea Coraddu [b,*], Luca Oneto [c]

[a] NAOME, Strathclyde University, 16 Richmond St, Glasgow G1 1XQ, United Kingdom
[b] Faculty of Mechanical, Maritime and Materials Engineering Delft University of Technology, Mekelweg 2, Delft 2628 CD, the Netherlands
[c] University of Genoa, Via Opera Pia, 11a, 16145 Genova, Italy

ARTICLE INFO

Keywords:
Ultimate Strength Reduction
Stiffened Panels
Residual Stress
Welding
Nonlinear Finite Element Methods
Data Driven Methods
Computationally Aware

ABSTRACT

Ultimate limit state (ULS) assessment examines the maximum load-carrying capacity of structures considering inelastic buckling failure. Contrary to the traditional allowable stress principle which is mainly based on experiences, the ULS assessment focuses on explicitly evaluating the structural safety margin and thus enables a consistent level of safety/risk between conventional and novel structural designs. Modern structures are usually designed as a network of plates and stiffeners (e.g., ship structures, offshore and onshore wind turbine, and land-based bridge) joined by welding which induces a residual stress field. Hence, predicting the ultimate strength reduction of stiffened panels caused by welding residual stress is a crucial problem addressed by many scholars with different approaches, among which the Nonlinear Finite Element Method (NLFEM) is the prevailing approach within the community of structural engineering. Unfortunately, the NLFEM has a high computational requirement which prevents its use in the design, appraisal, and optimisation phases of stiffened panels. To well approximate the nonlinear finite element method, a data-driven method is proposed in this paper, with a functional which is computationally expensive to build but computationally inexpensive to use allowing its application at design stage. Results obtained in different (i.e., interpolation and extrapolation) scenarios using data generated by a state-of-the-art NLFEM on a series of stiffened panels will support the proposed method.

1. Introduction

The design, appraisal, and optimisation of engineering structural systems critically rely on the rational choices of analysis methods and assessment criteria [1,2]. The traditional analysis methods in structural engineering are developed based on solid mechanics [3,4] (e.g., elasticity, plasticity, large deflection instability, fracture mechanics and impact mechanics). The equilibrium equation is derived and solved by analytical approaches [5–10] or numerical approximations [11–18] (e.g., Finite Difference and Finite Element Method, respectively FDM and FEM). The assessment criteria include the allowable stress principle and limit state design [19]. Traditional allowable stress principle is predominately based on past experiences and therefore its application should be limited to the conventional design. Recently, the limit state design has become the preferred approach as it explicitly evaluates the structural safety margin being also able to ensure a consistent level of safety/risk between the conventional and novel structural design [20]. A limit state is formally defined as the condition beyond which a particular structural member or the entire structure would fail to perform the designated function [21]. From the viewpoint of structural appraisal, four types of limit states are relevant [22]: the Serviceability Limit State (SLS), the Ultimate Limit State (ULS), the Fatigue Limit State (FLS), and the Accidental Limit State (ALS). The SLS concerns the excessive deflection, vibration, and noise of structures under normal loading scenarios [23]. The FLS deals with the occurrence of fatigue cracking due to stress concentration and damage accumulation or crack growth under repeated loading with relatively low stress intensity [24–26]. The ALS evaluates the widespread structural damage from accidents, such as collisions, grounding, explosion and fire [27–31].

When compared with the other types of limit states, the ULS assessment is the most relevant in terms of structural safety issues under extreme conditions [32,33]. In fact, ULS deals with the catastrophic

* Corresponding author.
E-mail addresses: shen.li@strath.ac.uk (S. Li), a.coraddu@tudelft.nl (A. Coraddu), luca.oneto@unige.it (L. Oneto).

https://doi.org/10.1016/j.engstruct.2022.114423
Received 13 July 2021; Received in revised form 20 April 2022; Accepted 15 May 2022

collapse of structures caused by excessive loading by examining the maximum load-carrying capacity (i.e., the ultimate strength) of a structural system considering inelastic buckling failure, with reference to the most probable extreme load case. Therefore, the ULS assessment is a mandatory phase in the design of large-scale structures, such as ships [34–39], offshore drilling platforms [40,41], floating wind turbines [42,43], box girder beams [44–46], and land-based civil structures [47–50]. In all the aforementioned engineering structures, stiffened panel formed of stiffeners and attached plating is one of the most common solutions of structural design [51–54]. The construction of stiffened panels is usually completed through welding: as a result initial imperfections are induced in the structures taking the form of geometric deflection and welding residual stress [55]. As shown by the comprehensive studies such as [56–61], the ultimate strength of stiffened panels is strongly influenced by the initial imperfections. The resulting geometric deflection and welding residual stress are predominantly caused by the heat imparted to the plating along the weld, typically fillet welds of attached stiffeners and butt welds between adjacent plates [55,62–64]. During the welding process, the rapid heating of the separate parts and subsequent cooling of the welded construction introduces a tensile stress zone close to the weld which is balanced by a compressive stress zone away from the weld [55].

The measurement of welding residual stress has always been an active research area. Pioneering works investigating the measurement of residual stress distribution and magnitude are documented in [56,57]. In these works, the distribution pattern of welding residual stress is assumed as rectangular blocks: a tensile stress field close to the intersection between the stiffeners and attached plates (e.g., welding line) and a compressive stress field at the central part of the plates achieving equilibrium. This distribution pattern simplifies the experimental observations and is generally accepted by the research community [32,55]. The very recent full-scale measurements [65–67] and numerical simulation [68] of welding-induced residual stress further confirm the rationality behind these idealised distributions. In terms of the magnitude of welding residual stress, empirical formulas were proposed by [69,70] to calculate the width of the tensile stress block b_t as a function of plating dimension, weld heat input, and weld leg length. However, the information regarding a specific welding technique (i.e., weld heat input and weld leg length) is usually not available at design stage. For this reason, a common solution is to employ the empirical formula introduced by [57] where the magnitude of compressive residual stress can be evaluated as a fraction of the material yield stress which is known at design stage.

When it comes to the effect of residual stress on ultimate strength of stiffened plated structures, it was argued that the cyclic loading experienced during operation (e.g., wave load) would lead to a relaxation of the built-in residual stress, i.e., shakedown effect. Hence, there is probably no need to consider residual stress in the structural integrity assessment. However, quantitative evidence for a wide spectrum of structural configurations is still lacking in terms of how much residual stress can be relieved. In addition, as shown in [71], whilst the residual stress can be shaken down, its mechanism is fairly complex and is dependent on the failure mode of the panels. Additionally, the reduction in residual stress is not uniform throughout the plate-stiffener combination. Hence, to make the design on the safe side, it was not recommended to consider the shakedown effect.

The ultimate strength reduction of stiffened panels under compression caused by welding residual stress has been investigated in several works [72–76]. The state-of-the-art solution for the analysis of ultimate strength reduction is the Nonlinear Finite Element Method (NLFEM) [77,60] thanks to its ability to evaluate all types of buckling failure modes and their complex interaction with other influential parameters, whereas the semi-analytical such as PULS [78] are dependent on certain assumptions in terms of the buckling modes and failure criteria (i.e., membrane stress yielding on certain locations). In addition, NLFEM allows a tractable inclusion/removal of the residual stress, whereas the simplified approaches such as [79–88] are not easily adaptable to take into account the effect of residual stress [89] because of the complexity of the relation between the strength reduction and structural configurations. Hence, NLFEM appears to be only dependable solution to deal with the effect of residual stress on stiffened plated structures. The FEM is a numerical approach to solve the boundary value problem for many engineering applications. The mathematical basis was first proposed by [90]. In terms of the ULS analysis, the nonlinear formulation of FEM (e.g., NLFEM) is adopted to account for the geometric and material nonlinearity. Unfortunately, while being robust for the current problem of interest, NLFEM is not the usual analysis method in the design, appraisal, and optimisation phases of stiffened panels because of its high computational requirements [91]. This fact raises significant challenges and limitations, both from the academic and industrial perspectives, for the reliability assessment and optimisation of large-scale structures considering the negative effects of residual stress [92–94]. As a consequence, currently, the potential impact of welding residual stress on the strength of stiffened panels is not mandatory in many structural design codes such as the IACS Common Structural Rules for shipbuilding [95,96].

For this purpose, in this work, we propose to overcome this limitation by exploiting a data-driven approach [97–99]. Data-driven methods (DDMs) allow to accurately approximate the NLFEM without requiring to design grounded simplifications. DDMs are able to automatically learn a functional representing the NLFEM using a series of data generated by running multiple times the NLFEM. The advantage of this approach is that the learned functional is computationally inexpensive to apply, addressing the limitations of the NLFEM. The disadvantage is that this function is computationally expensive to build. In fact, building a model using DDM requires running the NLFEM code multiple times to generate the data and then to train the functional with a Machine Learning (ML) algorithm. Nevertheless, once this procedure is completed, the resulting learned functional can be reused inexpensively as many times as necessary. Note that this approach has been already exploited in the past to resolve many solid mechanics related problems [100–111]. A number of surrogates have been developed in the literature to predict the buckling and ultimate strength of stiffened plated structures [80,112,83,113,114]. Some exploit the simple relation between panel slenderness ratio and ultimate strength (e.g., second-order polynomials), while some take the full set of geometric scantling and material property as the input. However, it has not yet been applied in predicting the ultimate strength reduction of stiffened panels caused by residual stress. For these reasons, we will first focus our attention on stiffened panels for the shipbuilding industry as they are the most common type of structures in this domain [115,116]. Then we will generate a database of simulations, using a state-of-the-art NLFEM, containing information on ultimate strength reduction for stiffened panels with different geometric dimensions and material properties. Subsequently, we will test the ability of the data-driven method to accurately learn the NLFEM considering two different and statistically consistent [117] scenarios: interpolation and extrapolation. In the interpolation scenario we will train the ML model considering a random subset of geometric dimensions and material properties keeping the remaining ones for testing. In the extrapolation scenario we will train the ML model considering a subset of the geometric dimensions and material properties in a specific range and we tested the resulting model for geometric dimensions and material properties outside the range exploited during the training phase. Since the no-free-lunch theorem [118] ensure us that there is no way to determine a priori the best ML model to use for a specific application, in this work we will test different state-of-the-art-methods (i.e., Kernel Methods [119], Ensemble Methods [120], Neural Networks [98], and Gaussian Processes [121]). Results on the two different scenarios will support the proposal and its potential for future use in the design, appraisal, and optimisation of engineering structural systems.

The rest of the paper is organised as follows. Section 2 will describe

the problem of estimating the ultimate strength reduction of stiffened panels caused by welding residual stress, numerical modelling and simulation by NLFEM, and the data generated by running multiple times the NLFEM. Section 3 will present our DDM to approximate the NLFEM using the generated data in the interpolation and extrapolation scenarios. Section 4 will report the result of applying the methodology presented in Section 3 using the data described in Section 2. Section 5 will conclude the paper.

2. Problem Description, NLFEM, and Generated Data

2.1. Problem Description

A typical stiffened panel with the definition of its geometric dimensions is reported Fig. 1. Considering this geometry, it is possible to define the nine parameters characterising the stiffened panel: plate length (a), plate width (b), plate thickness (t_p), stiffener web height (h_w), stiffener web thickness (t_w), stiffener flange width (b_f), stiffener flange thickness (t_f), material yield stress (σ_Y) and material Young's modulus (E).

Conventionally, two dimensionless parameter are employed to characterise the slenderness of a stiffened panel, i.e., plate slenderness ratio (β) and column slenderness ratio (λ) defined as follows

$$\beta = \frac{b}{t_p}\sqrt{\frac{\sigma_Y}{E}}, \tag{1}$$

$$\lambda = \frac{a}{\pi r}\sqrt{\frac{\sigma_{Yeq}}{E}}. \tag{2}$$

Note that r is the radius of gyration and σ_{Yeq} is the equivalent material yield stress of a stiffened panel's cross section. The nine basic geometric scantling and material property are employed as the input features, rather than the dimensionless slenderness ratio which were commonly adopted in simple surrogate development in this field. Simple surrogate with slenderness ratios as the only input appears to provide unsatisfactory prediction as shown in our preliminary work, which is likely due to the increased nonlinearity as compared with the well-studied relation between slenderness ratio and ultimate strength. Thus, this motivates us to exploit the advanced learning algorithms for predicting the reduction of ultimate strength based on nine basic design variables.

Regarding the magnitude of the welding residual stress (σ_{rcx}), an average-level of severity recommended in [56,57] is assumed for the compressive stress field, corresponding to the most common design specification as defined below

$$\sigma_{rcx} = 0.15\sigma_Y. \tag{3}$$

The magnitude of tensile stress (σ_{rtx}) is taken as the material yield stress (σ_Y) and the width of tensile field (b_t) is determined based on the equilibrium of initial tensile force and compressive force as follows.

$$2b_t\sigma_{rtx} = (b - 2b_t)\sigma_{rcx}, \tag{4}$$

We define the reduction factor (ζ) as the ratio between the ultimate compressive strength with welding residual stress σ_{xu}^{wR} and the ultimate compressive strength without welding residual stress σ_{xu}^{woR}

$$\zeta = \frac{\sigma_{xu}^{wR}}{\sigma_{xu}^{woR}}. \tag{5}$$

2.2. NLFEM

The NLFEM modelling adopted in this paper has been previously proposed in [89]. For the sake of completeness, this section will summarise it. As recommended by the International Ships and Offshore Structures Congress (ISSC) [122], a two-bay and two-span stiffened panel model has been adopted, as reported in Fig. 2. The longitudinal girders and transverse frames are modelled by constraining the out-of-plane movement. Symmetric boundary conditions are applied on four edges. The compressive load is imposed through a reference point in combination with a displacement-controlled method, such that the loaded edge keeps straight. The present model extent and boundary condition are able to account for the interaction between adjacent structures and eliminate the effect of the end-rotation of the stiffener, providing a rational representation of ship-type orthogonal grillage for ULS assessment.

In terms of the meshing scheme of the FEM, the general criteria is that the local plating is discretised by an even number of elements, while the characteristic element size is in the range of $[50, 100]$ millimetres. In this study, the local plate is discretised transversely with 10 elements, in which each tensile stress block is represented by 1 element and the central part is partitioned into 8 elements. In the longitudinal direction,

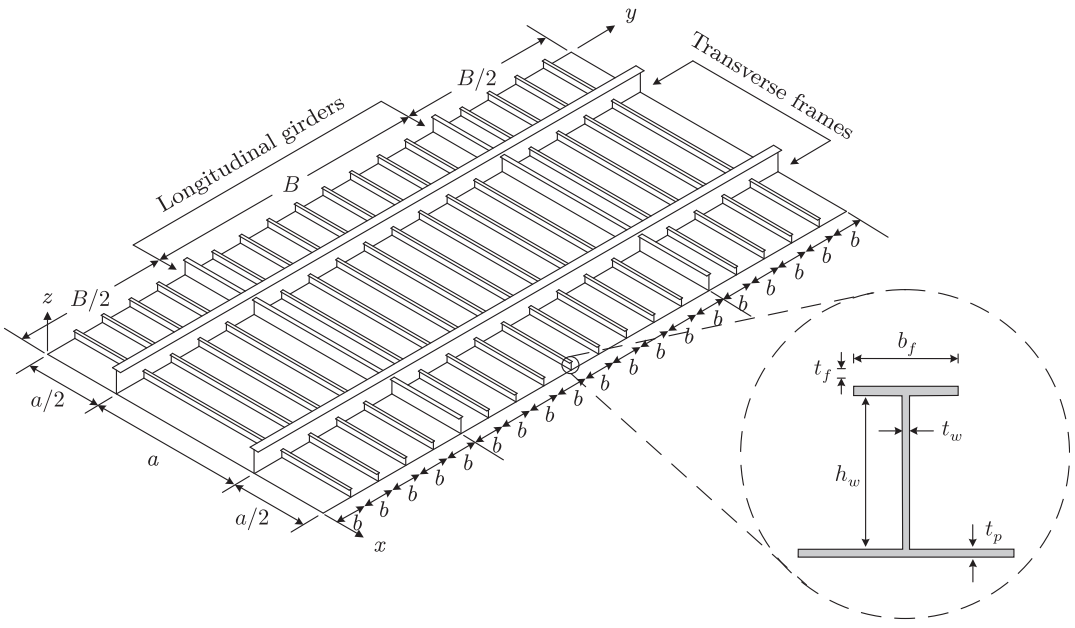

Fig. 1. Definition of geometric dimensions of a stiffened panel.

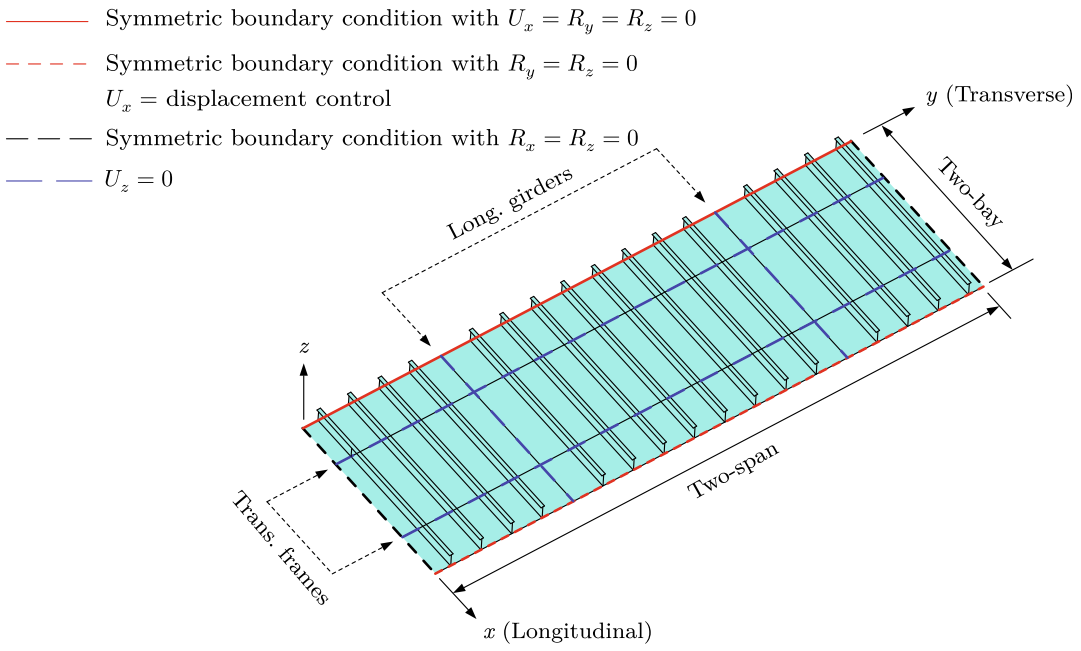

Fig. 2. Schematics of model extent and boundary condition.

the number of elements is calculated as 10-times of the closest round-off even number of the plating aspect ratio. Regarding the meshing of stiffeners, 6 elements are utilised in both stiffener web and flange regardless of their dimension. This is consistent with the ISSC approach [122].

An initial geometric imperfection is applied by the direct nodal translation approach through an external subroutine. Three different types of geometric imperfections are considered (i.e., local plate deflection w_{opl}, column-type deflection w_{oc}, and stiffener sideway deflection w_{os}) as follows

$$w_{opl} = w_{opl}^{max}\sin(\frac{m\pi x}{a})\sin(\frac{\pi y}{b}), \tag{6}$$

$$w_{oc} = w_{oc}^{max}\sin(\frac{\pi x}{a})\sin(\frac{\pi y}{B}), \tag{7}$$

$$w_{os} = w_{os}^{max}\frac{z}{h_w}\sin(\frac{\pi x}{a}). \tag{8}$$

A representation of the initial geometric imperfection is given by Fig. 3.

The maximum deflection magnitudes of each geometric imperfection type, w_{opl}^{max}, w_{oc}^{max}, and w_{os}^{max}, respectively for local plate deflection, column-type deflection, and stiffener sideway deflection, are defined as follows

$$w_{opl}^{max} = 0.1\beta^2 t_p, \tag{9}$$

$$w_{oc}^{max} = 0.0015a, \tag{10}$$

$$w_{os}^{max} = 0.0015a. \tag{11}$$

Examples of different types of initial deflections applied in finite element models are shown in Fig. 4. The welding residual stress is applied by defining the initial stress field of the finite element model. The commonly adopted distributions of residual stress include a hybrid distribution pattern (Fig. 5) proposed by [57], rectangular distribution pattern (Fig. 6) reported in [55], and bi-axial distribution pattern (Fig. 7) developed by [32]. In all these distribution patterns, the initial stress field in the attached plating is modelled by the rectangular strips. However, in the hybrid pattern, the stress field in the stiffener follows a

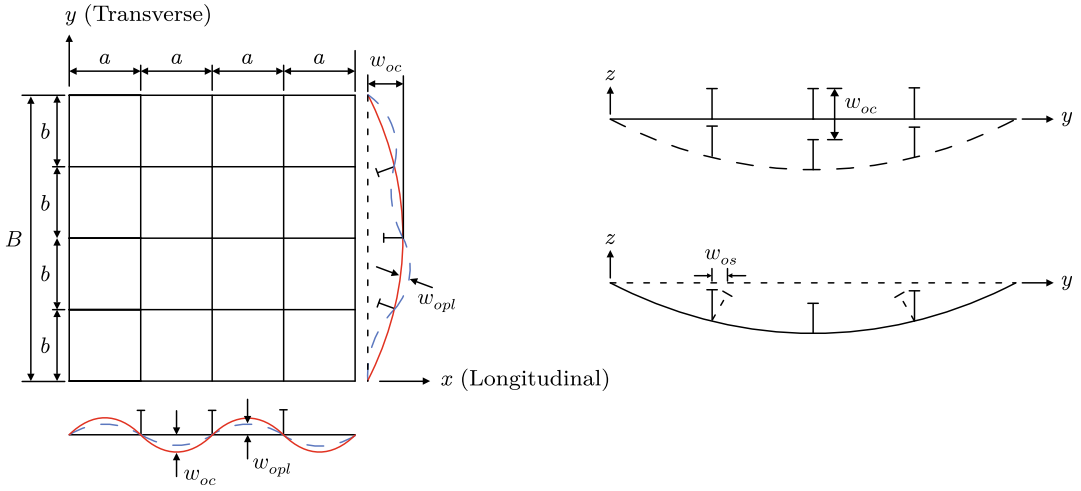

Fig. 3. Representation of the initial geometric imperfection (i.e., local plate deflection w_{opl}, column-type deflection w_{oc}, and stiffener sideway deflection w_{os}).

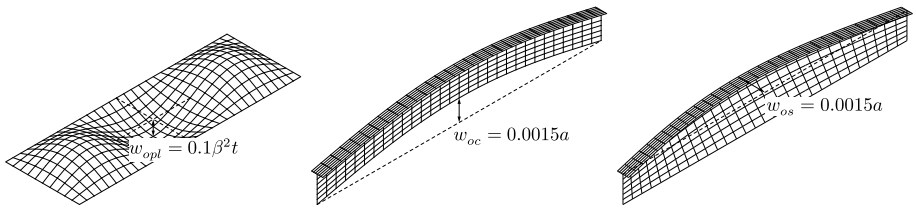

(a) Local plate defection. (b) Column type defection. (c) Stiffener sideway deflection.

Fig. 4. Examples of different types of initial deflections applied in finite element model.

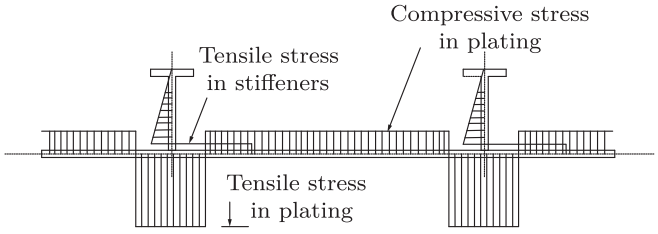

Fig. 5. Hybrid distribution pattern of welding residual stress.

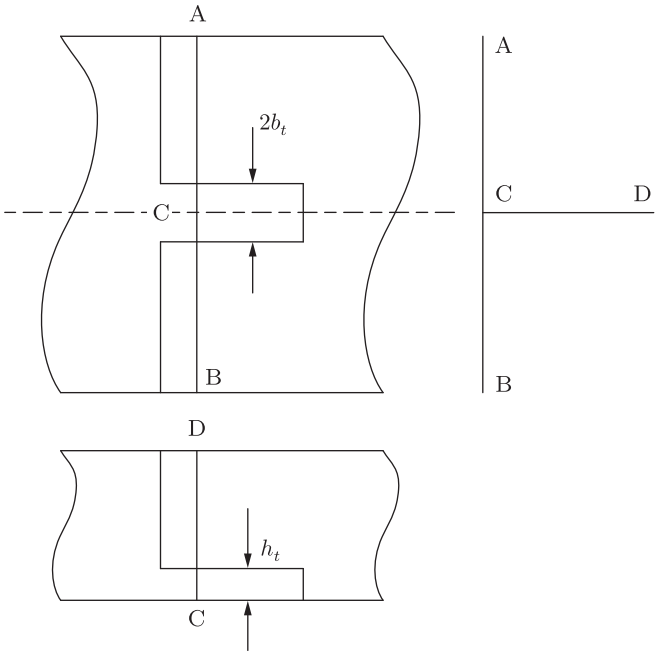

Fig. 6. Rectangular distribution pattern of welding residual stress.

triangular shape, as compared with the rectangular profile suggested by [55]. The triangular distribution pattern may only be appropriate for the analytical approach developed by [57], in which case the stiffeners are subdivided into many small fibres. However, in NLFEM, the overly fine mesh which is required for triangular shape modelling would lead to an excessively long computational time and possibly a convergence issue causing the failure of simulation [89]. Thus, this work follows the recommendation proposed by [55]. Regarding the bi-axial distribution suggested by [32], it would be important in the case of bi-aixial compression. Nevertheless, this is disregarded in the present work since the main focus is the longitudinal compression which is the most critical scenario for stiffened plated structures.

The tensile block is applied to the intersection between local plates and stiffeners, while the compressive block is applied to the remaining

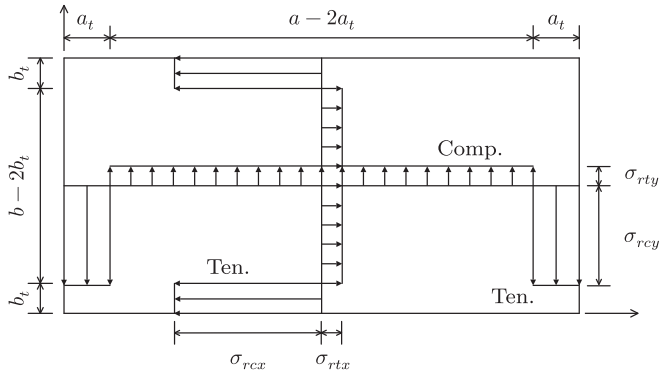

Fig. 7. Bi-axial distribution pattern of of welding residual stress.

part. The width of the tensile stress block is determined by assuming that the tensile residual stress equals the material yield stress, and the compressive residual stress corresponds to the average-level magnitude as given by Eq. (3). The ratio between the height of the tensile stress block h_t and the total web height h_w is

$$\frac{h_t}{h_w} = \frac{1}{6}, \tag{12}$$

so to satisfy the meshing scheme of stiffeners and to consider a value corresponding to the average-level severity. A relaxation step prior to any other external load application is utilised for the self-equilibrium of the initial stress field. It should be noted that the relaxation step would lead to a minor difference on the geometric imperfection as reported in [89]. However, the difference would be negligible, usually less than 0.5 millimetres [89]. The relaxation step aims to achieve a self-equilibrium of the applied stress field, which in some cases could help avoid the convergence issue of obtaining a numerical solution. A typical example of the stiffened panel after stress relief is reported in Fig. 8.

An example of the effects of residual stress on the progressive collapse behaviour (load-shortening curve) of slender and stocky stiffened panels predicted by NLFEM is reported in Fig. 9. Note that the high slenderness panel is of $\beta = 1.664$ and $\lambda = 0.729$ and the low slenderness panel is of $\beta = 1.167$ and $\lambda = 0.280$. In these load-shortening curves, the peak values correspond to the ultimate strength of stiffened panels in different conditions. The ultimate compressive strength without welding residual stress (σ_{xu}^{woR}) is highlighted with a solid black marker. The ultimate compressive strength with welding residual stress (σ_{xu}^{wR}) is indicated with a hollow marker. It is clear that an appreciable strength reduction is caused by the residual stress in stiffened panels with different slenderness.

2.3. Generated Data

In this section, we will describe the data generated with the NLFEM described in Section 2.2 for stiffened panel described in Section 2.1 for

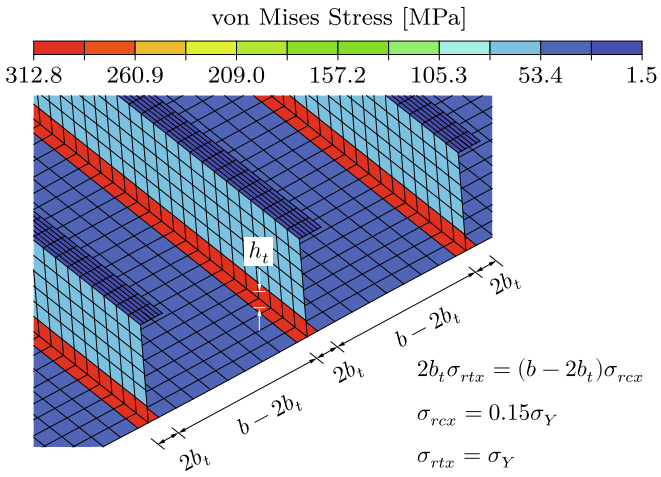

Fig. 8. Stiffened panel after stress relief.

different values of the parameters (geometry and material) characterising it (see Table 1).

The database contains 136 scenarios generated randomly in the ranges reported in Table 2 and Table 3. For the interpolation scenario, we sampled 100 points within the lower and upper limits of each input feature (see Table 2) according to the ISSC benchmark study [122] in order to represent typical configurations of stiffened panels for marine applications. For the extrapolation scenario, we sampled 12 points from each range reported in Table 3, considering ranges of 5%, 10%, and 15% outside the interpolation ranges, respectively. Both tee-bar and angle-bar stiffened panels are considered during the data sampling. Nevertheless, as shown in a previous study, the ultimate strength reduction caused by residual stress is nearly identical between tee-bar and angle-bar stiffened panels [89]. Hence, it should be reasonable to expect that the developed data-driven models are applicable to both tee-bar and angle-bar stiffened panels. Regarding the flat-bar stiffened panel, a different database is needed and is out of the scope of present research. For each of the 136 scenarios, the NLFEM has been run twice to compute ζ (see Eq. (5)). Each simulation took an average of 30 min on a machine equipped with two Intel Xeon Silver 4216, 128 GB of RAM, and 512 GB SSD running Windows Server 2019 and equipped with ABAQUS 2019 for a total of 136 h for creating the entire dataset. Note that significant man hours are also required for the modelling phase prior to each simulation. From these computational requirements, it is immediately clear why NLFEM is normally not exploited for the initial design, appraisal, and optimisation of structural engineering systems and why we propose DDMs to address these computational barriers.

Table 1
Parameters characterising the stiffened panel.

Parameter	Symbol	Unit
Plate length	a	mm
Plate width	b	mm
Plate thickness	t_p	mm
Stiffener web height	h_w	mm
Stiffener web thickness	t_w	mm
Stiffener flange width	b_f	mm
Stiffener flange thickness	t_f	mm
Material yield stress	σ_Y	MPa
Material Young's modulus	E	MPa

Table 2
Ranges for the LHS exploited to generate the data for the interpolation scenario.

Symbol	Interpolation Range
a	[2550 ÷ 4750]
b	[850 ÷ 950]
t_p	[8.5 ÷ 37]
h_w	[138 ÷ 580]
t_w	[9 ÷ 15]
b_f	[90 ÷ 150]
t_f	[12 ÷ 20]
σ_Y	[235 ÷ 315]
E	[20 ÷ 21]·10^4

3. Data Driven Models

The problem that we want to face in this work is to predict the result of the NLFEM (i.e., ζ) based on the input parameters reported in Table 2 using just the data produced by a number NLFEM simulations (see Section 2.3).

This problem can be easily mapped into a now-classical supervised ML problem, in particular an ML regression problem [97]. In regression, we have an input space $\mathscr{X} \subseteq \mathbb{R}^d$ composed of d features (in our case the 9 parameters of Table 1), an output space $\mathscr{Y} \subseteq \mathbb{R}$ (in our case the output of the NLFEM, namely ζ), and a series of n examples, a dataset, input/output relation $\mathscr{D}_n = \{(\boldsymbol{x}_1, y_1), \cdots, (\boldsymbol{x}_n, y_n)\}$ where $\boldsymbol{x}_i \in \mathscr{X}$ and $y_i \in \mathscr{Y}$ $\forall$ $i \in \{1, \cdots, n\}$. The scope is to learn the unknown input/output relation $\mu : \mathscr{X} \rightarrow \mathscr{Y}$ based just on $\mathscr{D}_n$. Generally μ is a probabilistic relation, but in our case, this relation is induced by the NLFEM so it is deterministic. An ML regression algorithm $\mathscr{A}$, characterised by its hyperparameters $\mathscr{H}$,

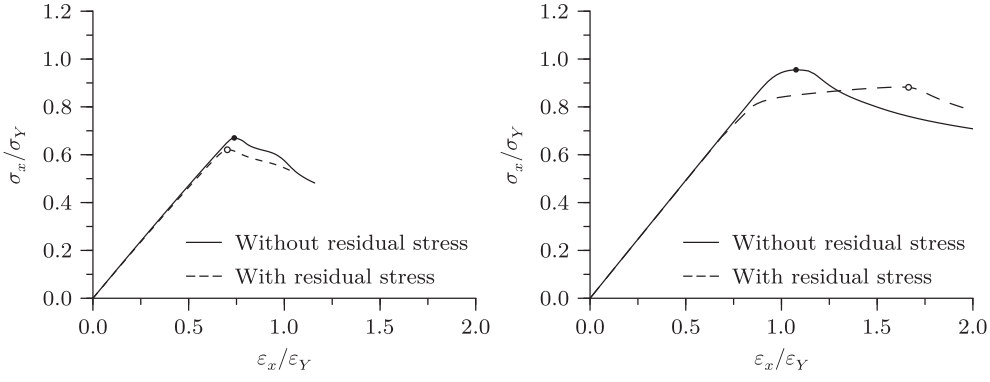

(a) High slenderness ratio. (b) Low slenderness ratio.

Fig. 9. Example of the effects of residual stress on the progressive collapse behaviour, represented by load-shortening curves, of slender and stocky stiffened panels predicted by NLFEM. σ_{xu}^{woR} is highlighted with a solid black marker and σ_{xu}^{wR} is indicated with a hollow marker.

Table 3
Ranges for the LHS exploited to generate the data for the extrapolation scenario.

Symbol	Extrapolation Range 5%	10%	15%
a	[2422.5 ÷ 2550], [4750 ÷ 4987.5]	[2295 ÷ 2422.5], [4987.5 ÷ 5225]	[2167.5 ÷ 2295], [5225 ÷ 5462.5]
b	[807.5 ÷ 850], [950 ÷ 997.5]	[765 ÷ 807.5], [997.5 ÷ 1045]	[722.5 ÷ 765], [1045 ÷ 1092.5]
t_p	[8.1 ÷ 8.5], [37 ÷ 38.9]	[7.7 ÷ 8.1], [38.9 ÷ 40.7]	[7.2 ÷ 7.7], [40.7 ÷ 42.6]
h_w	[131.1 ÷ 138], [580 ÷ 609]	[124.2 ÷ 131.1], [609 ÷ 638]	[117.3 ÷ 124.2], [638 ÷ 667]
t_w	[8.6 ÷ 9], [15 ÷ 15.8]	[8.1 ÷ 8.6], [15.8 ÷ 16.5]	[7.7 ÷ 8.1], [16.5 ÷ 17.3]
b_f	[85.5 ÷ 90], [150 ÷ 157.5]	[81 ÷ 85.5], [157.5 ÷ 165]	[76.5 ÷ 81], [165 ÷ 172.5]
t_f	[11.4 ÷ 12], [20 ÷ 21]	[10.8 ÷ 11.4], [21 ÷ 22]	[10.2 ÷ 10.8], [22 ÷ 23]
σ_Y	[223.3 ÷ 235], [315 ÷ 330.8]	[211.5 ÷ 223.3], [330.8 ÷ 346.5]	[199.8 ÷ 211.5], [346.5 ÷ 362.3]
E	$[19 \div 20]\cdot 10^4$, $[21 \div 22.05]\cdot 10^4$	$[18 \div 19]\cdot 10^4$, $[22.05 \div 23.1]\cdot 10^4$	$[17 \div 18]\cdot 10^4$, $[23.1 \div 24.15]\cdot 10^4$

selects a model f inside a set of possible ones $\mathscr{F}$ based on the available data $\mathscr{A}_{\mathscr{H}} : \mathscr{D}_n \times \mathscr{F} \rightarrow f$. $\mathscr{F}$ is generally unknown and depends on the choice of $\mathscr{A}$ and $\mathscr{H}$. Many different ML algorithms exist in the literature [97,98,123,124] but, as the no-free-lunch theorem states [118], there is no way to determine a priori the best ML algorithms to use for a specific application. For this reason, in this work (see Section 3.1) we will consider a series of different state-of-the-art ML algorithms. The error of f in approximating μ is measured by a prescribed metric $M : f \rightarrow \mathbb{R}$. Multiple metrics are available in the field of ML for regression [125], nonetheless, because of the physical meaning of ζ in this paper we will rely on three main metrics: Mean Absolute Error (MAE), Mean Absolute Percentage Error (MAPE), and the Pearson Correlation Coefficient (PCC). For the sake of selecting the best ML algorithms and the related optimal hyperparameters and to estimate (in both interpolation and extrapolation scenarios) the performance of the final model according to the desired metrics, a statistically consistent Model Selection (MS) and Error Estimation (EE) phase needs to be performed [117]. Section 3.2 will focus on addressing this tricky problem.

3.1. ML Models

In this section we briefly recall the four algorithms that we will exploit in this work by pointing out the idea behind them, how to use them, and their hyperparameters. The selected algorithms represent the most effective algorithms in the main four families of ML regression algorithms [97,97,98,123,124]: Kernel Methods [119], Ensemble Methods [120], Neural Networks [98], and Gaussian Processes [121].

3.1.1. Kernel Methods

Kernel Methods are a family of techniques which exploits the "Kernel trick" for distances in order to extend linear techniques to the solution of non-linear problems [126]. Kernel methods select the model which minimises the trade-off between the performance, measured with a defined metric, over the data and the complexity of the solution, measured with different measures of complexities [119,97]. Support Vector Regression (SVR) represents the most known and effective Kernel methods techniques. The hyperparameters of the SVR are: the kernel, which is usually fixed to be Gaussian because of the reasons described in [127], the kernel hyperparameter γ, which regulates the nonlinearity of the solution, and the regularisation hyperparameter C, which trades-off accuracy and complexity of the solution. C and γ need to be tuned during the MS phase.

3.1.2. Ensemble Methods

Ensemble Methods are methods based on the wisdom of the crowd principle [128]: construct many simple and independent models and then combine them to obtain a more complex and effective model [120] The Random Forests (RF) [129] are probably the most prominent algorithms between the Ensemble Methods. In RF the simple models are the Decision Trees (DT) [130]. The DT is a flowchart-like structure in which each internal node represents a test of a feature, each branch represents the outcome of the test, and each leaf node represents an output of the tree. A path from the root to a leaf represents a model rule. A DT is built with a recursive schema until it reaches its desired depth. Each node of the DT, starting from the root node, is built by choosing the attribute and the cut that most effectively splits the set of samples into two subsets based on the information gain. RF combines bagging with random subset feature selection. In bagging, each DT is independently constructed using a bootstrap sample of the dataset. RF adds an additional layer of randomness to bagging. In addition to constructing each DT using a different bootstrap sample of the data, RF changes how the DT are constructed. In standard DT, each node is split using the best division among all variables. In a RF, each node is split using the best among a subset of predictors randomly chosen at that node. Eventually, a simple majority vote is taken for prediction. The accuracy of the final model depends mainly on three different factors: 1) how many trees compose the forest, 2) the accuracy of each tree, and 3) the correlation between them. The accuracy for RF converges to a limit as the number of trees in the forest increases, while it rises as the accuracy of each tree increases and the correlation between them decreases. There are several hyperparameters which characterise the performance of the final model: the number of trees n_t, the number of samples to extract during the bootstrap procedure, the depth of each tree, the number of predictors n_p exploited in each subset during the growth of each tree, and finally the weights assigned to each tree. Nevertheless, in common applications, the RF sensitivity to these factors (apart from n_t and n_p) is quite low [131,129].

3.1.3. Neural Networks

Neural Networks are a family of techniques which combine many simple models of a human brain neuron, called perceptrons [132], in order to build a complex network. The neurons are organised in stacked layers connected by weights that are learned based on the available data via backpropagation [133]. If the architecture of neural networks consists of only one hidden layer, it is called shallow, while, if multiple layers are stacked together, the architecture is defined as deep. From a functional point of view both architectures have the same representation power [134] but in practice, for some applications like natural language processing and image analysis, deep networks outperform the shallow ones [98]. In our context, instead, where the number of samples is limited and features are not structured, it is more reasonable to use a shallow network [135,98]. In particular, in this work, we exploited a pretty well known and effective architecture, the The Multilayer Perceptron Network with Dropout (MLP) [135,98], where a single hidden layer is present, we train it with adaptive subgradient methods, and we tuned the following hyperparameters during the MS phase [98]: the number of neurons in the hidden layer n_h, the dropout rate p_d, the percentage of data to use as batch size p_b, the learning rate r_l, the fraction of gradient to keep at each step ρ, the learning rate decay r_d, and the activation function.

3.1.4. Gaussian Processes

Gaussian Processes are nonparametric Bayesian ML methods [121]. Gaussian Processes have several benefits: they work well on small datasets and have the ability to provide uncertainty measurements on the predictions. Unlike many popular supervised ML algorithms that learn exact values for every parameter of the model, the Bayesian approach infers a probability distribution over all possible values. The

Bayesian approach works by specifying a prior distribution on the parameters and relocating probabilities based on evidence (i.e., observed data) using Bayes' Rule [136]. The updated distribution, called the posterior distribution, thus incorporates information from both the prior distribution and the dataset. To get predictions at points of interest, the predictive distribution can be calculated by weighting all possible predictions by their calculated posterior distribution. The prior and likelihood is usually assumed to be Gaussian for the integration to be tractable. Using that assumption and solving for the predictive distribution, we get a Gaussian distribution, from which we can obtain a point prediction using its mean and an uncertainty quantification using its variance. Gaussian Process Regression (GPR) is nonparametric (i.e., not limited by a functional form), so rather than calculating the probability distribution of parameters of a specific function, GPR calculates the probability distribution over all admissible functions that fit the data. However, we specify a prior (on the function space), calculate the posterior using the training data, and compute the predictive posterior distribution on our points of interest. In GPR, we first assume a Gaussian process prior, which can be specified using a mean and covariance function. The form of the mean function and covariance kernel function in the GPR prior is chosen and tuned during MS. The mean function is typically constant, either zero or the mean of the training dataset. There are many options for the covariance kernel function: it can have many forms as long as it follows the properties of a kernel so also the kernel hyperparameter needs to be tuned during the MS phase. A popular kernel is the composition of the constant kernel with the radial basis function, this kernel has two hyperparameters: signal variance σ^2, and lengthscale l [121].

3.2. Model Selection and Error Estimation

MS and EE deal with the problem of tuning and assessing the performance of a ML algorithm [117]. Resampling techniques are commonly used by researchers and practitioners since they work well in most situations and this is why we will exploit them in this work. Other alternatives exist, based on the Statistical Learning Theory, but they tend to underperform resampling techniques in practice. Resampling techniques are based on a simple idea: the original dataset $\mathscr{D}_n$ is resampled once or many (n_r) times, with or without replacement, to build three independent datasets called learning, validation and test sets, respectively $\mathscr{L}_l^r$, $\mathscr{V}_v^r$, and $\mathscr{T}_t^r$, with $r \in \{1, \cdots, n_r\}$ such that

$$\mathscr{L}_l^r \cap \mathscr{V}_v^r = \emptyset, \quad \mathscr{L}_l^r \cap \mathscr{T}_t^r = \emptyset, \quad \mathscr{V}_v^r \cap \mathscr{T}_t^r = \emptyset \tag{13}$$

$$\mathscr{L}_l^r \cup \mathscr{V}_v^r \cup \mathscr{T}_t^r = \mathscr{D}_n \tag{14}$$

Subsequently, to select the best hyperparameters' combination $\mathscr{H}$ in a set of possible ones $\mathfrak{H} = \{\mathscr{H}_1, \mathscr{H}_2, \cdots\}$ for the algorithm $\mathscr{A}_{\mathscr{H}}$ or, in other words, to perform the MS phase, the following procedure has to be applied:

$$\mathscr{H}^* : \quad \underset{\mathscr{H} \in \mathfrak{H}}{\operatorname{argmin}} \sum_{r=1}^{n_r} M(\mathscr{A}_{\mathscr{H}}(\mathscr{L}_l^r), \mathscr{V}_v^r), \tag{15}$$

where $\mathscr{A}_{\mathscr{H}}(\mathscr{L}_l^r)$ is a model built with the algorithm $\mathscr{A}$ with its set of hyperparameters $\mathscr{H}$ and with the data $\mathscr{L}_l^r$, and where $M(f, \mathscr{V}_v^r)$ is a desired metric. Since the data in $\mathscr{L}_l^r$ are independent from the data in $\mathscr{V}_v^r$, $\mathscr{H}^*$ should be the set of hyperparameters which allows achieving a small error on a data set that is independent from the training set.

Then, to evaluate the performance of the optimal model which is $f_{\mathscr{A}}^* = \mathscr{A}_{\mathscr{H}^*}(\mathscr{D}_n)$ or, in other words, to perform the EE phase, the following procedure has to be applied:

$$M(f_{\mathscr{A}}^*) = \frac{1}{n_r} \sum_{r=1}^{n_r} M(\mathscr{A}_{\mathscr{H}^*}(\mathscr{L}_l^r \cup \mathscr{V}_v^r), \mathscr{T}_t^r). \tag{16}$$

Since the data in $\mathscr{L}_l^r \cup \mathscr{V}_v^r$ are independent from the ones in $\mathscr{T}_t^r$, $M(f_{\mathscr{A}}^*)$ is an unbiased estimator of the true performance, measured with the metric M, of the final model [117].

In this work we will rely on Complete k-fold cross validation which means setting $n_r \leqslant \binom{n}{k}\binom{n-\frac{n}{k}}{k}, l = (k-2)\frac{n}{k}, v = \frac{n}{k}$, and $t = \frac{n}{k}$ and the resampling must be done without replacement [117].

In our experiment, we investigated two different scenarios to understand the interpolation and extrapolation capability of the DDM:

- Interpolation Scenario: ML models will be trained considering a random subset of geometric dimensions and material properties keeping the remaining ones for testing;
- Extrapolation Scenario: ML models will be trained considering a subset of geometric dimensions and material properties in a specific range and the resulting models will be tested for geometric dimensions and material properties outside the range exploited during the training phase, as reported in Table 3.

Therefore, the two scenarios just differ in the definition of the three sets $\mathscr{L}_l^r$, $\mathscr{V}_v^r$, and $\mathscr{T}_t^r$, which are the subset of data exploited for building, tuning, and testing the models. For the Interpolation scenario $\mathscr{L}_l^r$, $\mathscr{V}_v^r$, and $\mathscr{T}_t^r$ have been created by simply randomly selecting data from $\mathscr{D}_n$. For the Extrapolation scenario $\mathscr{L}_l^r$, $\mathscr{V}_v^r$, and $\mathscr{T}_t^r$ have been created by putting in $\mathscr{L}_l^r$ a subset of the geometric dimensions and material properties in a specific range, in $\mathscr{V}_v^r$ a subset of the geometric dimensions and material properties outside the rage used for $\mathscr{L}_l^r$, and in $\mathscr{T}_t^r$ a subset of the geometric dimensions and material properties outside the range used for $\mathscr{L}_l^r$ and $\mathscr{V}_v^r$.

4. Experimental Results

In this section we will show the results of applying the methods of Section 3 on the dataset of Section 2.

4.1. Experimental Setting

In this section we recall the pipeline of our approach and the parameter exploited in the experiments:

1. construction of the dataset as defined in Section 2.3;
2. definition of the regression tasks, namely predict the reduction factor ζ (see Eq. (5)) based on the varying parameters (geometrical and material) of the stiffened panels considered in Section 2 (see Table 1);
3. for each one of the considered ML algorithms (SVR, RF, MLP, and GPR in Section 3.1) we built a model using the MS strategy defined in Section 3.2 where we set the number of fold $k = 10$ and $n_r = 1000$, and we performed the EE phase described in the very same section. For the MS we searched the hyperparameters using the following ranges:
   - SVR: $\mathscr{H} = \{C, \gamma\}$ and $\mathfrak{H} = 10^{\{-6.0,-5.8,\cdots,4.0\}} \times 10^{\{-6.0,-5.8,\cdots,4.0\}}$;
   - RF: we set $n_t = 3000$ (since increasing it did not improve the results) and $\mathscr{H} = \{n_p\}$ with $\mathfrak{H} = \{1, \cdots, 9\}$;
   - MLP: $\mathscr{H} = \{n_h, p_d, p_b, r_l, \rho, r_d\}$ and $\mathfrak{H} = \{5, 10, 20, 40, 80, 160, 320, 640, 1280\} \times \{0, 0.001, 0.01, 0.1\} \times \{0.01, 0.1, 1\} \times \{0.001, 0.01, 0.1, 1\} \times \{0.9, 0.09\} \times \{.001, .01, .1, 1\}$ and as activation function we used the RELU one [98];
   - GPR: $\mathscr{H} = \{\sigma^2, l\}$ and $\mathfrak{H} = 10^{\{-6.0,-5.8,\cdots,4.0\}} \times 10^{\{-6.0,-5.8,\cdots,4.0\}}$.

For the interpolation scenario, as described in Section 3.2 we simply randomly selected the data from 100 simulation inserted in $\mathscr{D}_n$ (see Section 2.3) to generate $\mathscr{L}_l^r$, $\mathscr{V}_v^r$, and $\mathscr{T}_t^r$ with $r \in \{1, \cdots, n_r\}$. For the extrapolation scenario, instead, we considered the 100 simulation

inserted in $\mathscr{D}_n$ to generate $\mathscr{L}_l^r$, $\mathscr{V}_v^r$ while $\mathscr{T}_t^r$ contains the data from the 5%, 10%, and 15% extrapolation ranges (see Section 2.3).

Experiments have been repeated 30 times reporting mean and standard deviation of MAPE, MAE, and PCC on $\mathscr{T}_t^r$.

Results are reported in Table 4. The proposed methods show very high accuracy in predicting the reduction of ULS (i.e., ζ) both in the interpolation and extrapolation scenarios.

4.2. Interpolation Scenario

In this scenario, ML models try to predict the reduction factor ζ in various, but different, configurations of the design parameters, as discussed in Section 2.3, within the ones exploited for building the models. In other words, this scenario is accounting for configurations that belong inside the search space used to build the dataset, i.e., within the range reported in Table 2. In particular, from Table 4 it is possible to observe that DDMs show a high accuracy for predicting the ultimate strength reduction of stiffened panels caused by residual stress, as indicated by the mean values of three performance indices (i.e., MAPE, MAE and PCC). In particular, SVR is the most performing DDM among the four ML algorithms with a MAPE error of about 1.5%. The high accuracy of the experiments is repeatable as demonstrated by the acceptably small standard deviation of performance indices.

4.3. Extrapolation Scenario

In this second scenario, the DDMs based on all ML algorithms try to predict the reduction factor ζ in various, but different, configurations of the design parameters, with respect to those exploited for building the model, considering configurations that belong outside of the search space used to build the dataset, i.e., within the ranges 5%, 10%, and 15% reported in Table 3. From Table 4 it is possible to observe that as expected, the extrapolation scenarios have seen higher prediction errors as compared with those in the interpolation scenario. Considering the most performing ML algorithm (SVR) the results report an increase of the MAPE error from $1.6\% \pm 0.2\%$ to $2.4\% \pm 0.2\%$ for the 5% scenario, to $2.8\% \pm 0.4\%$ for the 10% scenario, and to $4.2\% \pm 0.5\%$ for the 15% scenario. Also in this scenario, the SVR is still the best performing algorithm for the current problem, which is consistent with the results obtained in the interpolation scenario. Moreover, with a larger extrapolation range, the performance of the DDMs gradually declined. Finally, also in this scenario, all experiments retain a good repeatability as indicated by the relatively small standard deviation, while they also tend to grow with the extrapolation range.

Table 4
Predict the reduction of ULS: MAPE, MAE, and PCC of SVR, RF, MLP, and GPR for the Interpolation and Extrapolation Scenario.

Method	Int.	Ext.		
		5%	10%	15%
		MAPE		
SVR	1.6 ± 0.2	2.4 ± 0.2	2.8 ± 0.4	4.2 ± 0.5
RF	2.0 ± 0.2	2.8 ± 0.2	3.4 ± 0.3	5.0 ± 0.5
MLP	2.8 ± 0.2	4.0 ± 0.3	4.8 ± 0.2	7.1 ± 0.3
GPR	2.6 ± 0.1	3.8 ± 0.3	4.5 ± 0.3	6.7 ± 0.5
		MAE		
SVR	$.009 \pm .001$	$.011 \pm .001$	$.018 \pm .001$	$.036 \pm .003$
RF	$.011 \pm .001$	$.013 \pm .001$	$.022 \pm .002$	$.043 \pm .004$
MLP	$.015 \pm .001$	$.019 \pm .001$	$.031 \pm .002$	$.061 \pm .004$
GPR	$.014 \pm .001$	$.018 \pm .001$	$.029 \pm .002$	$.058 \pm .003$
		PCC		
SVR	0.89 ± 0.10	0.85 ± 0.09	0.81 ± 0.08	0.78 ± 0.10
RF	0.85 ± 0.11	0.81 ± 0.08	0.77 ± 0.07	0.74 ± 0.09
MLP	0.76 ± 0.12	0.72 ± 0.07	0.69 ± 0.08	0.66 ± 0.07
GPR	0.78 ± 0.08	0.75 ± 0.09	0.71 ± 0.09	0.69 ± 0.07

5. Conclusions

In this paper, we focused on assessing the ultimate limit state to evaluate the maximum load-carrying capacity of structures considering inelastic buckling failure. The ultimate limit state is an indicator of the structural performance under extreme conditions and is adopted to formulate the structural safety margin within the limit state design framework. It, therefore, enables a consistent level of safety/risk between conventional and novel structural designs, contrary to the traditional allowable stress principle, which is mainly based on experiences and then applicable just to conventional structures. Predicting the ultimate strength reduction of stiffened panels caused by welding residual stress is a crucial problem addressed in the past by many scholars with different approaches. The Nonlinear Finite Element Method is the common approach within the community of structural engineering. Unfortunately, this method cannot be efficiently used in the design, appraisal, and optimisation phases of stiffened panels because of its high computational requirement. For this purpose, in this work, we estimated the strength reduction computed by the Nonlinear Finite Element Method with a data-driven model. The latter, based on a series of Nonlinear Finite Element Method outputs corresponding to stiffened panels characterised by different geometries and material properties, proved to be able to synthesise the complex related functional. The resulting function, while computationally expensive to build, is computationally inexpensive to use and then it can be leveraged to design, to appraise, and to optimise stiffened panels.

Results obtained taking into account two different scenarios (i.e., interpolation and extrapolation) proved and supported the proposed computationally inexpensive method for its application at design stage. In fact, for the interpolation scenario the most performing data-driven model was able to reach accuracy of $\approx 99\%$. Moreover, for the more challenging extrapolation scenario, characterised by 15% outside the interpolation ranges, the most performing data-driven model was able to reach an accuracy close to $\approx 96\%$.

This work is surely a promising first step toward enforcing the inclusion of the potential impact of welding residual stress in a code-based strength assessment for stiffened panel's structural design (e.g., in the IACS Common Structural Rules for shipbuilding), even if more in-depth tests (using also different structures) need to be performed. Moreover, in the future, we plan to include this data-driven model within an optimisation framework, to optimise the structural design of various stiffened plated structures considering the impact of the welding residual stress.

Besides, it is recommended that a more in-depth research is needed to advance the understanding on the shakedown phenomenon and to quantify the relaxation of residual stress in relation to service time. If such knowledge is developed, the present data-driven models can be extended by introducing more scenarios considering different severities of residual stress, i.e., introducing additional input features, so as to incorporate the consideration of shakedown.

In terms of the impact on the design guidance development, a direct incorporation of the developed data-driven models with design code such as CSR may be difficult, as a closed-form explicit formula is preferred. However, the main strength of the developed tool is its high accuracy and computational efficiency, which makes it an ideal alternative to the direct computation by NLFEM. Hence, the developed model appears to be a highly capable tool for advancing the research in buckling and ultimate strength of stiffened plated structures considering residual stress. This may ultimately lead to the specification of partial safety factors in CSR explicitly related to residual stress.

Declaration of Competing Interest

The authors declare that they have no known competing financial

interests or personal relationships that could have appeared to influence the work reported in this paper.

References

[1] Sechler EE, D.L.G. Airplane structural analysis and design, John Wiley & Sons; 1944.
[2] Hughes O, P.J.K. Ship structural analysis and design. Soc Naval Archit Marine Eng; 2013.
[3] Timoshenko S. Strength of materials. 3rd ed. CBS; 2004.
[4] Timoshenko S, Goodier J. Theory of elasticity. 3rd edition. McGraw-Hill; 1970.
[5] Zhou Y, Xia Y, Fujino YZ. Analytical formulas of beam deflection due to vertical temperature difference. Eng Struct 2021;240:112366.
[6] Timoshenko S, Woinowsky-Krieger S. Theory of plates and shells. 2nd edition. McGraw-Hill; 1970.
[7] Liu SW, Ziemian RD, Chen L. C.S.L., Bifurcation and large-deflection analyses of thin-walled beam-columns with non-symmetric open-sections. Thin-Wall Struct 2018;132: 287–301.
[8] Kołakowski Z, Mania RJ. Semi-analytical method versus the fem for analysis of the local post-buckling of thin-walled composite structures. Comput Struct 2013; 97:99–106.
[9] Chang LZ, Messali F, Esposito R. Capacity of unreinforced masonry walls in out-of-plane two-way bending: A review of analytical formulations. Structures 2020; 28:2431–47.
[10] Paik JK, Kim DK, Lee H, Shim YL. A method for analyzing elastic large deflection behavior of perfect and imperfect plates with partially rotation-restrained edges. J Offshore Mech Arct Eng 2012;134(2):021603.
[11] de Lima Araújo D, Azevedo Coelho S, Regina Mesquita de Almeida S, Khalil El Debs M. Computational modelling and analytical model for two-step corbel for precast concrete system. Eng Struct 2021;244:112699.
[12] Liu LL, Liu AR, Fu JY, Lu HW, Pi YL, Bradford MA. Flexural-torsional buckling of shear deformable steel circular arches under a central concentrated load in a thermal environment. Eng Struct 2021;242:112505.
[13] Cook R, Malkus DS, Plesha ME, Witt RJ. Concepts and applications of finite element analysis, John Wiley & Sons. 4th ed. 2002.
[14] Benson S, Collette MD. Finite element methods and approaches. Encyclopedia Maritime Offshore Eng.
[15] Amatya I, Seo JW, Jeong E, Lee J. Numerical study for structural performance evaluation of adhesively bonded aluminum dynamic message signs. Thin-Wall Struct 2021;107193.
[16] Karpenko O, Oterkus S, Oterkus E. An in-depth investigation of critical stretch based failure criterion in ordinary state-based peridynamics. Int J Fract 2020;226: 97–119.
[17] Karpenko O, Oterkus S, Oterkus E. Influence of different types of small-size defects on propagation of macro-cracks in brittle materials. J Peridynam Nonlocal Model 2020;2:289–316.
[18] Karpenko O, Oterkus S, Oterkus E. Peridynamic investigation of the effect of porosity on fatigue nucleation for additively manufactured titanium alloy ti6al4v. Theoret Appl Fract Mech 2021;112:102925.
[19] Lee DH, Kim SJ, Lee MS, Paik JK. Ultimate limit state based design versus allowable working stress based design for box girder crane structures. Thin-Wall Struct 2019;134:491–507.
[20] Trahair NS. Limit states design of crane runway girders. Eng Struct 2021;240: 112395.
[21] Wong MB. Plastic Analysis and Design of Steel Structures. Elsevier; 2009.
[22] Paik JK. Advanced structural safety studies: with extreme conditions and accidents. Springer; 2020.
[23] Jia JB, Paik JK. Engineering Dynamics and Vibrations. CRC Press; 2018.
[24] Braun M, Fischer C, Fricke W, Ehlers S. Extension of the strain energy density method for fatigue assessment of welded joints to sub-zero temperatures. Fatigue Fract Eng Mater Struct 2020;43:2867–82.
[25] Braun M, Fischer C, Fricke W, Ehlers S. Fatigue strength of fillet-welded joints at subzero temperatures. Fatigue Fract Eng Mater Struct 2020;43:403–16.
[26] Kim DK, Incecik A, Choi HS, Wong EWC, Yu SY, Park KS. A simplified method to predict fatigue damage of offshore riser subjected to vortex-induced vibration by adopting current index concept. Ocean Eng 2018;157:401–11.
[27] Yu ZL, Amdahl J. A numerical solver for coupled dynamic simulation of glacial ice impacts considering hydrodynamic-ice-structure interaction. Ocean Eng 2021; 226:108827.
[28] Yu ZL, Amdahl J, Sha Y. Large inelastic deformation resistance of stiffened panels subjected to lateral loading. Mar Struct 2018;59:342–67.
[29] Sha Y, Hao H. Nonlinear finite element analysis of barge collision with a single bridge pier. Eng Struct 2012;41:63–76.
[30] Sha Y, Hao H. Laboratory tests and numerical simulations of barge impact on circular reinforced concrete piers. Eng Struct 2013;46:593–605.
[31] Benson S, AbuBakar A, Dow RS. A comparison of computational methods to predict the progressive collapse behaviour of a damaged box girder. Eng Struct 2013;48:266–80.
[32] Paik JK. Ultimate limit state analysis and design of plated structures. Wiley Online Library 2018.
[33] Van Pham P, Mohareb M, Fam A. Numerical and analytical investigation for ultimate capacity of steel beams strengthened with GFRP plates. Eng Struct 2021; 243:112668.
[34] Kim DK, Kim BJ, Seo JW, Kim HB, Zhang XM, Paik JK. Time-dependent residual ultimate longitudinal strength - grounding damage index (r-d) diagram. Ocean Eng 2014;76:163–71.
[35] Li S, Hu ZQ, Benson S. Progressive collapse analysis of ship hull girders subjected to extreme cyclic bending. Mar Struct 2020;102803.
[36] Li S, Benson S. A re-evaluation of the hull girder shakedown limit states. Ships Offshore Struct 2019;14(sup 1):239–50.
[37] Georgiadis DG, Samuelides MS, Li S, Kim DK, B.S. Influence of stochastic geometric imperfection on the ultimate strength of stiffened panel in compression. In: 8th International conference on marine structures; 2021.
[38] Li S, Hu ZQ, Benson S. Bending response of a damaged ship hull girder predicted by the cyclic progressive collapse method. In: 8th International conference on collision and grounding of ships and offshore structures; 2019.
[39] Li S, Hu ZQ, Benson S. A cyclic progressive collapse method to predict the bending response of a ship hull girder. In: 7th International conference on marine structures; 2019.
[40] Asgarian B, Lesani M. Pile-soil-structure interaction in pushover analysis of jacket offshore platforms using fiber elements. J Constr Steel Res 2009;65:209–18.
[41] Mohd MH, Zalaya MA, Latheef M, Choi HS, Rahman MAA, Kim DK. Ultimate bending capacity of aged fixed platform by considering the effect of marine fouling. Latin Am J Solids Struct 2019;16:1–12.
[42] Yeter B, Garbatov Y, Soares CG. Numerical and experimental study of the ultimate strength of a monopile structure. Eng Struct 2019;194:290–9.
[43] Dimopoulos CA, Gantes CJ. Experimental investigation of buckling of wind turbine tower cylindrical shells with opening and stiffening under bending. Thin-Wall Struct 2012;54:140–55.
[44] Sharifi Y, P.J.K. Ultimate strength reliability analysis of corroded steel-box girder bridges. Thin-Wall Struct 2011;49: 157–166.
[45] Li S, Benson S, Dow RS. A timoshenko beam finite element formulation for thin-walled box girder considering inelastic buckling. In: 8th International conference on marine structures; 2021.
[46] Jasion P, Pawlak A, Paczos P. Buckling and post-buckling behaviour of selected cold-formed c-beams with atypical flanges. Eng Struct 2021;244:112693.
[47] Mohabeddine A, Koudri YW, Correia JAFO, Castro JM. Rotation capacity of steel members for the seismic assessment of steel buildings. Eng Struct 2021;244: 112760.
[48] Wang YH, Richard Liew JY, Lee SC. Ultimate strength of steel-concrete-steel sandwich panels under lateral pressure loading. Eng Struct 2016;115:96–106.
[49] Kim TS, Kuwamura H, Kim S, Lee Y, Cho T. Investigation on ultimate strength of thin-walled steel single shear bolted connections with two bolts using finite element analysis. Thin-Wall Struct 2009;47:1191–202.
[50] Brubak L, Andersen H, Hellesland J. Ultimate strength prediction by semi-analytical analysis of stiffened plates with various boundary conditions. Thin-Wall Struct 2013;62:28–36.
[51] Doan VT, Liu B, Garbatov Y, Wu WG, Guedes Soares C. Strength assessment of aluminium and steel stiffened panels with openings on longitudinal girders. Ocean Eng 2020;200:107047.
[52] Li S, Hu ZQ, Benson S. An analytical method to predict the buckling and collapse behaviour of plates and stiffened panels under cyclic loading. Eng Struct 2019; 109627.
[53] Tanaka D, Yanagihara A, Yasuoka M, Harada S, Okazawa M, Fujikubo T. Yao, Evaluation of ultimate strength of stiffened panels under longitudinal thrust. Mar Struct 2014;36:21–50.
[54] Shanmugam NE, ZDQ., Choo YS, Arockiaswamy M. Experimental studies on stiffened plates under in-plane load and lateral pressure. Thin-Wall Struct 2014; 80: 22–31.
[55] Yao T, Fujikubo M. Buckling and ultimate strength of ship and ship-like floating structures. Butterworth-Heinemann; 2016.
[56] Smith CS, Davidson PC, Chapman JC. Strength and stiffness of ships' plating under in-plane compression and tension. Trans RINA 1987;130:277–93.
[57] Smith CS, Anderson N. Strength of stiffened plating under combined compression and lateral pressure. Trans RINA 1991;134:131–47.
[58] Benson S, Downes J, Dow RS. Ultimate strength characteristics of aluminium plates for high-speed vessels. Ships Offshore Struct 2011;6:67–80.
[59] Benson S, Downes J, Dow RS. Load shortening characteristics of marine grade aluminium alloy plates in longitudinal compression. Thin-Wall Struct 2013;70: 19–32.
[60] Gordo J. Effect of initial imperfections on the strength of restrained plates. J Offshore Mech Arct Eng 2015;137:051401.
[61] Ringsberg JW, Darie I, Nahshon K, Shilling G, Vaz MA, Benson S, Brubak L, Feng GQ, Fujikubo M, Gaiotti M, Hu ZQ, Jang BS, Paik JK, Slagstad M, Tabri K, Wang YK, Wiegard B, Yanagihara D. The issc 2022 committee iii.1-ultimate strength benchmark study on the ultimate limit state analysis of a stiffened plate structure subjected to uniaxial compressive loads. Mar Struct 2021;79:103026.
[62] Tekgoz M, Garbatov Y, Guedes Soares C. Ultimate strength assessment of welded stiffened plates. Eng Struct 2015;84:325–39.
[63] Chen BQ, Guedes Soares C. Effects of plate configurations on the weld induced deformations and strength of fillet-welded plates. Mar Struct 2016;50:243–59.
[64] Chen BQ, Hashemzadeh M, Guedes Soares C. Numerical and experimental studies on temperature and distortion patterns in butt-welded plates. Int J Adv Manuf Technol 2014;72(5):1121–31.
[65] Yi MS, Hyun CM, Paik JK. Full-scale measurements of welding-induced initial deflections and residual stresses in steel-stiffened plate structures. International Journal Maritime Engineering 2018;160(A4):504.
[66] Yi MS, Hyun CM, Paik JK. Three-dimensional thermo-elastic-plastic finite element method modeling for predicting weld-induced residual stresses and distortions in

steel stiffened-plate structures. World Journal of Engineering and Technology 2018;6:176–200.
[67] Yi MS, Noha SH, Lee DH, Seo DH, Paik JK. Direct measurements, numerical predictions and simple formula estimations of welding-induced biaxial residual stresses in a full-scale steel stiffened plate structure. Structures 2020;29: 2094–105.
[68] Chen BQ, Soares CG. Experimental and numerical investigation on welding simulation of long stiffened steel plate specimen. Marine Structures 2021;75: 102824.
[69] Yao T. Compressive ultimate strength of structural members in ship structure. PhD thesis. Japan: Osaka University; 1980.
[70] Yi MS, Hyun CM, Paik JK. An empirical formulation for predicting welding-induced biaxial compressive residual stresses on steel stiffened plate structures and its application to thermal plate buckling prevention. Ships and Offshore Structures 2019;14(sup 1):18–33.
[71] Gannon LG, Pegg NG, Smith MJ, Liu Y. Effect of residual stress shakedown on stiffened plate strength and behaviour. Ships Offshore Struct 2013;8(6):638–52.
[72] Gannon L, Liu Y, Pegg N, Smith MJ. Effect of welding-induced residual stress and distortion on ship hull girder ultimate strength. Mar Struct 2012;28:25–49.
[73] Gannon L, Liu Y, Pegg N, Smith MJ. Effect of three-dimensional welding-induced residual stress and distortion fields on strength and behaviour of flat-bar stiffened panels. Ships Offshore Struct 2013;8:565–78.
[74] Gannon L, Liu Y, Pegg N, Smith MJ. Nonlinear collapse analysis of stiffened plates considering welding-induced residual stress and distortion. Ships Offshore Struct 2016;11:228–44.
[75] Guo ZF, Bai RX, Lei ZK, Jiang H, Zou JC, Yan C. Experimental and numerical investigation on ultimate strength of laser-welded stiffened plates considering welding deformation and residual stresses. Ocean Eng 2021;234:109239.
[76] Li S, Benson S. The effects of welding-induced residual stress on the buckling collapse behaviours of stiffened panels. In: 5th International Conference on Maritime Technology and Engineering; 2020.
[77] Khan I, Zhang SM. Effects of welding-induced residual stress on ultimate strength of plates and stiffened panels. Ships Offshore Struct 2011;6:297–309.
[78] Byklum E, Steen E, Amdahl J. A semi-analytical model for global buckling and postbuckling analysis of stiffened panels. Thin-Wall Struct 2004;42(5):701–17.
[79] Paik JK, Thayamballi AK. An empirical formulation for predicting the ultimate compressive strength of stiffened panels. In: Proceedings of 7th International Offshore and Polar Engineering Conference, Honolulu, USA; 1997. p. 25–30.
[80] Kim DK, Lim HL, Kim MS, Hwang OJ, Park KS. An empirical formulation for predicting the ultimate strength of stiffened panels subjected to longitudinal compression. Ocean Eng 2017;140:270–80.
[81] Kim DK, Lim HL, Yu SY. Ultimate strength prediction of $\mathscr{T}$-bar stiffened panel under longitudinal compression by data processing: A refined empirical formulation. Ocean Eng 2019;192:106522.
[82] Kim DK, Yu SY, Lim HL, Cho NK. Ultimate compressive strength of stiffened panel: An empirical formulation for flat-bar type. J Mar Sci Eng 2020;8:605.
[83] Pu Y, Mesbahi E. Application of artificial neural networks to evaluation of ultimate strength of steel panels. Eng Struct 2006;28:1190–6.
[84] Zhang SM, Kkan I. Buckling and ultimate capability of plates and stiffened panels in axial compression. Marine Struct 2009;22:791–808.
[85] Ok D, Pu Y, Incecik A. Artificial neural networks and their application to assessment of ultimate strength of plates with pitting corrosion. Ocean Eng 2007; 34:2222–30.
[86] Ahmadi F, Ranji AR, Nowruzi H. Ultimate strength prediction of corroded plates with center-longitudinal crack using fem and ann. Ocean Eng 2020;206:107281.
[87] Anyfantis K. Ultimate strength of stiffened panels subjected to non-uniform thrust. Int J Naval Archit Ocean Eng 2020;12:325–42.
[88] Xu MC, Song ZJ, Zhang BW, Pan J. Empirical formula for predicting ultimate strength of stiffened panel of ship structure under combined longitudinal compression and lateral loads. Ocean Eng 2018;162:161–75.
[89] Li S, Kim DK, Benson S. The influence of residual stress on the ultimate strength of longitudinally compressed stiffened panels. Ocean Eng 2021;108839.
[90] Courant R. Variational methods for the solution of problemsof equilibrium and vibrations. Bull Am Math Soc 1943;49:1–23.
[91] Benson S, Downes J, Dow RS. Overall buckling of lightweight stiffened panels using an adapted orthotropic plate method. Eng Struct 2015;85:107–17.
[92] Li S, Kim DK, Benson S. A probabilistic approach to assess the computational uncertainty of ultimate strength of hull girders. Reliab Eng Syst Saf 2021;107688.
[93] Li S, Benson S. Probabilistic evaluation of the computational uncertainty in ultimate ship hull strength prediction. In: 5th International conference on maritime technology and engineering; 2020.
[94] Li S, Hu ZQ, Benson S. The sensitivity of ultimate ship hull strength to the structural component load-shortening curve. In: in: The 30th International Ocean and Polar Engineering Conference; 2020.
[95] IACS, Common structural rules for bulk carriers and oil tankers; 2019.
[96] IACS, Longitudinal strength standard for container ships; 2015.
[97] Shalev-Shwartz S, Ben-David S. Understanding machine learning: From theory to algorithms. Cambridge University Press; 2014.
[98] Goodfellow I, Bengio Y, Courville A, Bengio Y. Deep learning. MIT press Cambridge; 2016.
[99] Shin D, Kim YY. Data-driven approach for a one-dimensional thin-walled beam analysis. Comput Struct 2020;231:106207.
[100] Pizarro PN, Massone LM. Structural design of reinforced concrete buildings based on deep neural networks. Eng Struct 2021;241:112377.
[101] Li ZX, Zhang XJ, Shi YC, Wu CQ, Li J. Predication of the residual axial load capacity of CFRP-strengthened rc column subjected to blast loading using artificial neural network. Eng Struct 2021;242:112519.
[102] Almustafa MK, N.M.L. Machine learning prediction of structural response for frp retrofitted rc slabs subjected to blast loading, Eng Struct 2021;244: 112752.
[103] Huang PF, Chen ZY. Deep learning for nonlinear seismic responses prediction of subway station. Eng Struct 2021;244:112735.
[104] Bomarito GF, Townsend TS, Stewart KM, Esham KV, Emery JM, Hochhalter J. Development of interpretable, data-driven plasticity models with symbolic regression. Comput Struct 2021;252:106557.
[105] Jung S, Ghaboussi J. Neural network constitutive model for rate-dependent materials. Comput Struct 2006;84:955–63.
[106] Xiao SP, Deierling P, Attarian S, Tuhami A. Machine learning in multiscale modeling of spatially tailored materials with microstructure uncertainties. Comput Struct 2021;249:106511.
[107] Jokar J, Semperlotti F. Finite element network analysis: A machine learning based computational framework for the simulation of physical systems. Comput Struct 2021;247:106484.
[108] Eggersmann R, Stainier L, Ortiz M, Reese S. Efficient data structures for model-free data-driven computational mechanics. Comput Methods Appl Mech Eng 2021;382:113855.
[109] Eggersmann R, Kirchdoerfer T, Reese S, Stainier L, Ortiz M. Model-free data-driven inelasticity. Comput Methods Appl Mech Eng 2019;350:81–99.
[110] Kirchdoerfer T, Ortiz M. Data-driven computational mechanics. Comput Methods Appl Mech Eng 2016;304:81–101.
[111] Kirchdoerfer T, Ortiz M. Data driven computing with noisy material data sets. Comput Methods Appl Mech Eng 2017;326:622–41.
[112] Papanikolaou N, Anyfantis K. Construction of surrogate models for predicting the buckling strength of stiffened panels through doe and rsm methods. Eng Comput 2022;39(4):1374–406.
[113] Kim DK, Li S, Lee JR, Poh BY, Benson S, Cho NK. An empirical formula to assess ultimate strength of initially deflected plate: Part 1 = propose the general shape and application to longitudinal compression. Ocean Eng 2022;111151.
[114] Kim DK, Li S, Yoo K, Danasakaran K, Cho NK. An empirical formula to assess ultimate strength of initially deflected plate: Part 2 = combined longitudinal compression and lateral pressure. Ocean Eng 2022;111112.
[115] Putranto T, Körgesaar M, Jelovica J, Tabri K, Naar H. Ultimate strength assessment of stiffened panel under uni-axial compression with non-linear equivalent single layer approach. Mar Struct 2021;78:103004.
[116] Romanin L, Ferro P, Berto F. A simplified non-linear numerical method for the assessment of welding induced deformations. Mar Struct 2021;78:102982.
[117] Oneto L. Model Selection and Error Estimation in a Nutshell. Springer; 2020.
[118] Wolpert DH. The supervised learning no-free-lunch theorems. Soft Comput Industry 2002:25–42.
[119] Shawe-Taylor JS, Cristianini N. Kernel methods for pattern analysis. Cambridge University Press; 2004.
[120] Zhou Z-H. Ensemble methods: foundations and algorithms. CRC Press; 2012.
[121] Rasmussen CE. Gaussian processes in machine learning. Springer; 2003.
[122] ISSC, Ultimate strength. In: Proceedings of the 18th International Ship and Offshore Structures Congress, Rostock, Germany; 2012. p. 285–364.
[123] Fernández-Delgado M, Cernadas E, Barro S, Amorim D. Do we need hundreds of classifiers to solve real world classification problems? J Mach Learn Res 2014;15 (1):3133–81.
[124] Wainberg M, Alipanahi B, Frey BJ. Are random forests truly the best classifiers? J Mach Learn Res 2016;17(1):3837–41.
[125] Aggarwal CC. Data mining: the textbook. Springer; 2015.
[126] Scholkopf B. The kernel trick for distances. In: Advances in neural information processing systems; 2001. p. 301–7.
[127] Keerthi SS, Lin CJ. Asymptotic behaviors of support vector machines with gaussian kernel. Neural Comput 2003;15(7):1667–89.
[128] Yi SKM, Steyvers M, Lee MD, Dry MJ. The wisdom of the crowd in combinatorial problems. Cognit Sci 2012;36(3):452–70.
[129] Breiman L. Random forests. Mach Learn 2001;45(1):5–32.
[130] Rokach L, Maimon OZ. Data mining with decision trees: theory and applications. World scientific; 2008.
[131] I. Orlandi, L. Oneto, D. Anguita, Random forests model selection, in: European Symposium on Artificial Neural Networks, Computational Intelligence and Machine Learning, 2016, pp. 441–446.
[132] Rosenblatt F. The perceptron: a probabilistic model for information storage and organization in the brain. Psychol Rev 1958;65(6):386.
[133] Rumelhart DE, Hinton GE, Williams RJ. Learning representations by back-propagating errors. Cognit Model 1988;5(3):1.
[134] Cybenko G. Approximation by superpositions of a sigmoidal function. Math Control Signals Syst 1989;2(4):303–14.
[135] Bishop CM. Neural networks for pattern recognition. Oxford University Press; 1995.
[136] Bolstad WM, Curran JM. Introduction to Bayesian statistics. John Wiley & Sons; 2016.